FED-Vol. 190, Cavitation and Gas-Liquid Flow
in Fluid Machinery and Devices
ASME 1994

ROTORDYNAMIC FORCES IN CAVITATING INDUCERS

**Abhijit Bhattacharyya, Allan J. Acosta, Christopher E. Brennen,
and Thomas K. Caughey**
Division of Engineering and Applied Sciences
California Institute of Technology
Pasadena, California

ABSTRACT

This paper reports an experimental investigation of the rotordynamic forces that occur in a whirling three bladed inducer under the influence of cavitation. The effect of lowering the flow coefficient (and thus causing reverse flows) on these forces were also investigated. The results show the occurrence of large destabilizing peaks in the force tangential to the whirl orbit for positive whirl frequency ratios. Cavitation caused these forces to become destabilizing at both negative and positive whirl frequency ratios. The magnitude of the destabilizing forces increased with decreasing cavitation numbers and flow coefficient. The rotordynamic data obtained do not exhibit the kind of quadratic functional behavior which is normally assumed in many rotordynamic models. Consequently the conventional generalized stiffness, damping and inertia matrices cannot be determined for the inducer. The results demonstrate the complexity of rotordynamic forces and their consequences on stability of axial flow inducers.

NOMENCLATURE

A_i	Inlet cross-sectional area, πr_t^2
$[A]=\begin{bmatrix} A_{xx} & A_{xy} \\ A_{yx} & A_{yy} \end{bmatrix}$	Hydrodynamic force matrix, nondimensionalized by $\rho\pi\Omega^2 r_t^2 l$
F_o	Steady lateral force on the inducer
F_{ox}, F_{oy}	Components of the steady lateral force in the (X,Y) reference frame
F_x, F_y	Components of the instantaneous lateral forces in the (X,Y) reference frame, nondimensionalized by $\rho\pi\Omega^2 r_t^3 l$
F_n, F_t	Components of the time averaged force on the inducer which are normal and tangential to the whirl orbit respectively and are, nondimensionalized by $\rho\pi\Omega^2 r_t^3 l$
l	Axial blading length of the inducer
p_i	Inlet static pressure
p_v	Vapor pressure
Δp_t	Total pressure rise between inlet and outlet
Q	Flow rate
r_t	Inducer tip radius
u_t	Inducer tip speed, $r_t\Omega$
x, y	Instantaneous coordinates of the inducer center in the fixed reference frame, nondimensionalized by r_t
$\dot{x}, \dot{y}$	Time derivatives of x and y, nondimensionalized by $r_t\Omega$
$\ddot{x}, \ddot{y}$	Acceleration, nondimensionalized by $r_t\Omega^2$
$[K]=\begin{bmatrix} K_{xx} & K_{xy} \\ K_{yx} & K_{yy} \end{bmatrix}$	Generalized stiffness matrix, nondimensionalized by $\rho\pi\Omega^2 r_t^2 l$

$[C]=\begin{bmatrix} C_{xx} & C_{xy} \\ C_{yx} & C_{yy} \end{bmatrix}$ Generalized dampin g matrix, nondimensionalized by $\rho\pi\Omega r_t^2 l$

$[M]=\begin{bmatrix} M_{xx} & M_{xy} \\ M_{yx} & M_{yy} \end{bmatrix}$ Generalized inertia matrix, nondimensionalized by $\rho\pi r_t^2 l$

Symbols

ε	Radius of the whirl orbit, nondimensionalized by r_t
ρ	Density of the working fluid (water)
σ	Cavitation number, $\dfrac{(p_i - p_v)}{\frac{1}{2}\rho u_t^2}$
ω	Frequency of whirl motion
Ω	Inducer rotational frequency
ψ	Head coefficient, $\Delta p_t/(\rho u_t^2)$

INTRODUCTION

The purpose of the research presented in this paper is to obtain an insight into the characteristics of fluid-induced rotordynamic forces acting on an axial flow inducer operating under cavitating conditions. Rotordynamic forces arise when the inducer is displaced off-center and whirls in an orbit and are conventionally decomposed into forces normal and tangential to this whirl orbit. These forces can be destabilizing (depending on whirl speeds and operating conditions) and this paper presents experimental dynamic force data for varying whirl speeds, flow coefficients and cavitation numbers. The experiments have been conducted at the Rotor Force test facility (RFTF) at the California Institute of Technology. An experimental perturbation technique has been used to obtain steady and unsteady force data on a whirling inducer using a rotating force dynamometer for varying conditions of cavitation, flow rates and whirl. The perturbation is introduced in the form of a circular whirl motion created by an offset of the inducer center with respect to the housing centerline. The data presented are for a simple three bladed helical inducer with a blade angle of 9^o at the tip. The hydrodynamic force matrix obtained could be used to study the stability of the inducer.

A survey of literature shows a lack of dynamic force data on whirling cavitating inducers. Some of the early measurements of hydrodynamic radial forces includes a study by Rosenmann (1965) on a three bladed cavitating inducer. Karyeaclis et al. (1989) conducted previous experiments at the RFTF on a four bladed SEP (Société Européenne de Propulsion) inducer. Internal flows in inducers change substantially with flow coefficients. One such change is the appearance of reverse flow. These reverse flows occur both upstream as tip clearance leakage flows and downstream as re-entrant flow on the hub. The internal blade passage flows become highly complex and three dimensional (Lakshminarayana, 1972, 1982; Acosta, 1993; Bhattacharyya et al., 1993). It has also been shown that upstream swirling backflow can induce instability in the system through low cycle system oscillations (Kamijo et al. 1977); however the force data reported in this paper were taken at operating conditions at which such oscillations were not observed.

The results of the current experiments show the effect of flow coefficient and cavitation number on the rotordynamic and lateral forces and the range of whirl/shaft speed ratios (or whirl frequency ratios) over which they are destabilizing. The results also show a non-quadratic behavior of these forces with the whirl/shaft speed ratio as a consequence of which the conventional rotordynamic stiffness, damping and inertia coefficients cannot be obtained.

EXPERIMENTAL PROCEDURE

Experiments were conducted in the RFTF to obtain steady (lateral) and unsteady (rotordynamic) force data on a three bladed helical inducer. The important features of the inducer are that the hub/tip ratio and the helix pitch are 0.4 and 5.04 cm./revolution respectively and are constant. The blade angle is 9^o at the tip and the inducer has a swept back leading edge. The inducer is mounted on a rotating force dynamometer, used to measure all the components of the forces in a rotating frame. The data acquisition is done in such a manner as to correlate the position of the impeller with the forces measured. The inducer (along with the dynamometer) are mounted on a set of eccentric bearings which enable the inducer to be whirled in a circular motion in addition to its rotation. The radius of this whirl orbit can be set to different eccentricities (ε). A separate whirl motion is used in the system to impose this whirl motion. The electronic motor controls of the main motor (which rotates the inducer) and the whirl motor (which causes the whirl motion) operate such that the motor speeds are integral multiples of a fundamental frequency generated externally. This scheme allows the whirl motion to be driven at fractions of the main shaft frequency. Further details of the test facility and data acquisition and reduction can be found in Jery (1986) and Franz (1989).

A brief overview of the data reduction process is presented here; further details can be obtained from Jery (1986). The components of the instantaneous forces on a whirling inducer and the reference frames are shown in figure 1. The instantaneous force matrix $[F]$ can be expressed as the sum of a steady force matrix $[F_0]$ and a rotordynamic force matrix $[A]$:

$$\begin{bmatrix} F_x \\ F_y \end{bmatrix} = \begin{bmatrix} F_{ox} \\ F_{oy} \end{bmatrix} + \frac{\varepsilon}{R}\begin{bmatrix} A_{xx} & A_{xy} \\ A_{yx} & A_{yy} \end{bmatrix}\begin{bmatrix} \cos\omega t \\ \sin\omega t \end{bmatrix} \qquad (1)$$

The components of the rotordynamic matrix $[A]$ for a circular whirl orbit are such that $A_{xx} = A_{yy}$ and $A_{xy} = -A_{yx}$ as required by rotational invariance. This has also been

shown experimentally (from previous studies such as the one reported by Jery (1986)).

The forces normal to the whirl orbit (F_n) and tangential to the whirl orbit (F_t) can then be expressed as :

$$F_n = \frac{1}{2}(A_{xx} + A_{yy}) = A_{xx} = A_{yy} \tag{2}$$

and

$$F_t = \frac{1}{2}(A_{yx} - A_{xy}) = -A_{xy} = A_{yx} \tag{3}$$

The sign conventions are such that F_n is positive outward and F_t is positive in the direction of rotation. It follows that a *positive* tangential force is destabilizing when the whirl motion is in the same direction as the shaft rotational motion (i.e. a positive whirl/shaft speed ratio). Conversely, a negative F_t tends to stabilize the whirl motion for a positive whirl/shaft speed ratio. Likewise, a positive F_t would be stabilizing for a *negative* whirl motion. In the case of the normal force, a positive (outward) force could be considered as a destabilizing force in the sense that it tends to increase the radius of the whirl orbit.

Rotordynamicists typically characterize these forces in terms of inertia, stiffness and damping matrices for stability analysis in the following manner:

$$\begin{bmatrix} F_x \\ F_y \end{bmatrix} = \begin{bmatrix} F_{ox} \\ F_{oy} \end{bmatrix} - [K]\begin{bmatrix} x \\ y \end{bmatrix} - [C]\begin{bmatrix} \dot{x} \\ \dot{y} \end{bmatrix} - [M]\begin{bmatrix} \ddot{x} \\ \ddot{y} \end{bmatrix} + \text{higher order terms} \tag{4}$$

The matrices [K], [C] and [M] are the stiffness, damping and inertia matrices respectively. It can be shown that the components of the rotordynamic force matrix [A] can also be expressed in terms of the components of the stiffness, damping and inertia matrices as:

$$A_{xx} = M_{xx}\left(\frac{\omega}{\Omega}\right)^2 - C_{xy}\left(\frac{\omega}{\Omega}\right) - K_{xx} \tag{5}$$

$$A_{xy} = M_{xy}\left(\frac{\omega}{\Omega}\right)^2 + C_{xx}\left(\frac{\omega}{\Omega}\right) - K_{xy} \tag{6}$$

$$A_{yx} = M_{yx}\left(\frac{\omega}{\Omega}\right)^2 - C_{yy}\left(\frac{\omega}{\Omega}\right) - K_{yx} \tag{7}$$

$$A_{yy} = M_{yx}\left(\frac{\omega}{\Omega}\right)^2 + C_{yx}\left(\frac{\omega}{\Omega}\right) - K_{yy} \tag{8}$$

where ω is the whirl speed and Ω is the inducer rotational speed.

The above formulation implies that the coefficients of the stiffness, damping and inertia matrices can be obtained from rotordynamic force data if the forces can be expressed as a quadratic function of ω/Ω. Rotordynamic forces in centrifugal pumps, for example, do indeed show a quadratic variation of the forces with ω/Ω (Jery (1986), Franz (1989)). Recent studies of rotordynamic forces due to leakage flows have also shown such a quadratic relation (Guinzburg, 1992). The research presented in this paper investigates whether the rotordynamic forces on an inducer also show a quadratic behavior with ω/Ω and the manner in which these forces are affected by cavitation.

It should be noted that the data presented in this paper represent purely fluid induced forces in the sense that the effects of tare forces (the dry weight of the inducer and the centrifugal forces arising by running the inducer in air) have been subtracted from the total force. The steady and unsteady forces presented are mean values obtained by integration over many cycles of rotation and whirl. The normal force (F_n) and the tangential force (F_t) are normalized by $\rho\pi\Omega^2 r_t^2 l\varepsilon$. The steady forces ($F_o$ with components F_{ox} and F_{oy}) are normalized by $\rho\pi\Omega^2 r_t^2 l$ where ρ is the density of the fluid, r_t is the inducer tip radius (5.06 cm.) and l is the axial blading length (2.413 cm. in this case).

TEST MATRIX

The effects of cavitation were studied at two flow coefficients, $\phi = 0.074$ and $\phi = 0.049$. The flow coefficient (ϕ) is defined as the ratio of the local axial velocity to tip speed $\phi = Q/(u_t A_i)$ where Q is the flow rate and A_i is the inlet area ($A_i = \pi r_t^2$). The specific flow coefficients were chosen in order to study the effects of flow reversals on the forces ($\phi = 0.049$) and to compare these with the forces at a flow coefficient for which no flow reversals are observed ($\phi = 0.074$). Upstream and downstream flow reversals on this inducer have been studied previously and reported by Bhattacharyya et al., 1993.

For the set of experiments presented in this paper, the eccentricity is set at $\varepsilon = 0.0254$ cm. As a result of this eccentricity the clearance between the inducer blade tip and the housing varies between 0.028 cm. and 0.079 cm. A constant shaft rotational speed of 3000 rpm was used and the whirl speed was varied from -0.55 to +0.55 times the shaft speed

The tests on the inducer were conducted in water. The water was deaerated for several hours before conducting cavitation tests to reduce the air content to less than 3 ppm. The facility includes the pressure regulation system which allows operation at different suction pressures, p_i. A conventional cavitation number, σ, is used to define the non-dimensional suction conditions:

$$\sigma = \frac{(p_i - p_v)}{\frac{1}{2}\rho u_t^2} \tag{9}$$

where p_v is the vapor pressure (at the water temperature) and u_t is the tip speed of the inducer ($u_t = \Omega r_t$). The results presented are for various cavitation numbers.

RESULTS

Cavitation Performance

The cavitation characteristics of the inducer used for the current experiments are shown in figure 2 at $\phi = 0.074$ and $\phi = 0.049$ (3000 rpm). The head coefficient, ψ, defined as the ratio $\Delta p_t/(\rho u_t^2)$ where Δp_t refers to the change in the total pressure, is plotted against various values of σ at non-cavitating and cavitating conditions. In the case of $\phi = 0.074$, it is seen that as the cavitation number is reduced from non-cavitating values, the head coefficient started decreasing at $\sigma = 0.147$. However, there was a slight increase in the head coefficient at $\sigma = 0.113$ followed by a continuous head breakdown below $\sigma = 0.106$. The head coefficient is approximately 0.081 under non-cavitating conditions and $\psi = 0.077$ at $\sigma = 0.106$ (which represents a 4.9% head loss). The cavitation characteristics at $\phi = 0.049$ exhibit a similar behavior.

Steady forces due to cavitation

The results of the steady radial force measurements at $\phi = 0.074$ are presented in figure 3 for various whirl/shaft speed ratios (-0.55 to +0.55). The steady forces remain constant for a given cavitation number over the range of whirl/shaft speed ratios, but decrease with cavitation number. It is observed that the non-cavitating steady forces are much larger than the steady forces with cavitation; reasons for this are discussed later but it should be observed that previous research (Bhattacharyya et al. 1992) has shown that the presence of the downstream asymmetry inherent to the system causes large lateral forces.

Figure 4 shows the variation of the steady force for various whirl ratios at the flow coefficient of $\phi = 0.049$. The results differ from those obtained for $\phi = 0.074$ in that the cavitating forces are about the same magnitude as the non-cavitating forces. The large lateral forces at $\phi = 0.049$ are possibly due to the occurrence of reverse flows downstream of the inducer in the presence of a downstream aymmetry inherent to the system. Under these conditions, the steady force due to the effect of cavitation cannot be distinguished from the non-cavitating steady force.

Rotordynamic forces due to cavitation

The rotordynamic forces on the inducer were also obtained at various flow coefficients and cavitation numbers. The tangential force is plotted against whirl frequency ratio, ω/Ω, for $\phi = 0.074$ in figure 5. The significant result obtained is the occurrence of multiple zero crossings. There are some significant differences compared to the non-cavitating forces characteristics. One of these is that the tangential force remains negative in a significant region of negative whirl (it may be recalled that a negative tangential force in the negative whirl region is destabilizing). In fact for $\sigma = 0.106$ and $\phi = 0.074$, the tangential force does not reach a positive value in the negative whirl region (for the range of whirl/shaft speed ratios tested). Another feature of the tangential force is that it exhibits a positive peak in a range of positive whirl frequency ratio around at $\omega/\Omega \approx 0.2$. Such a peak is not observed in the non-cavitating tangential force at this flow coefficient (when there is no backflow). In fact, the magnitude of this peak increases in magnitude as the cavitation number is reduced. The location of the peak also tends to shift to lower whirl/shaft speed ratios. Thus, the extent and the manner in which the tangential forces become destabilizing depend on the extent to which the inducer cavitates. At larger positive whirl frequency ratios (especially for $\omega/\Omega > 0.4$), however, the tangential force is observed to become increasingly negative (and hence stabilizing) for decreasing cavitation numbers. Thus, for this case, destabilizing tangential forces are generally observed from $\omega/\Omega = 0.0$ to $\omega/\Omega \approx 0.4$ and in the region $\omega/\Omega < 0.0$.

Figure 6 presents the corresponding results for a flow coefficient $\phi = 0.049$. The variations with whirl frequency ratio are very much similar to those at $\phi = 0.074$, especially in the occurrence of a positive, destabilizing peak around $\omega/\Omega \approx 0.2$. Multiple zero crossings are also evident. However, at this flow coefficient, the tangential force continues to be destabilizing at $\omega/\Omega = 0.55$ for a cavitation number $\sigma = 0.098$ unlike F_t at $\omega/\Omega = 0.55$ for $\phi = 0.074$ (at the same cavitation number).

Figure 7 presents a comparison between the forces at the two flow coefficients for $\sigma = 0.106$. Note that the magnitude of the tangential force clearly increases with a decrease in the flow coefficient. In the region of negative whirl however, the forces become more stabilizing (except for the region between $\omega/\Omega = -0.5$ and $\omega/\Omega \approx -0.3$). The peak in the force in the region of positive whirl increases in magnitude (by approximately 200%). The location of this peak also shifts from $\omega/\Omega = 0.3$ at $\phi = 0.074$ to $\omega/\Omega = 0.2$ at $\phi = 0.049$. Another important observation is that for higher positive whirl ratios ($\omega/\Omega > 0.5$), the tangential forces tend to become increasingly destabilizing for the lower flow coefficient (whereas they become stabilizing for the higher flow coefficient).

Similar data for cavitation number of 0.098 is shown in figure 8. Again a positive peak of the tangential force occurs at $\omega/\Omega = 0.3$. For the lower flow coefficient, the range of destabilizing tangential force decreases for negative whirl (approximately $-0.3 < \omega/\Omega < -0.1$ at $\phi = 0.049$ compared to approximately $-0.4 < \omega/\Omega < 0.1$ at $\phi = 0.074$ for $\sigma = 0.098$).

The normal forces on the inducer at the flow coefficient of 0.074 have been plotted for different cavitation numbers in figure 9. It is observed that the normal forces do not vary significantly with cavitation number once cavitation has been established. However, compared to the non-cavitating data, we observe large and increasingly positive (destabilizing) normal forces with increasing positive whirl frequency ratios. Furthermore, the normal force in the presence of cavitation tends to be of a larger (negative) magnitude than the non-cavitating normal force for the range of whirl frequency ratios between -0.1 and +0.1. The characteristics of the normal force (with cavitation) in the region of negative whirl ($\omega/\Omega < -0.1$) tends to be similar to the non-cavitating normal force behavior.

Figure 10 presents similar data for the lower flow coefficient of 0.049. In this case the normal force behavior displays multiple zero crossings. A significant feature is the occurrence of negative peaks at all the cavitation numbers (including the non-cavitating case). It is also noted that the normal force decreases for $\omega/\Omega < -0.4$ and increases for $\omega/\Omega > +0.4$ with decreasing cavitation numbers.

The normal forces at a given cavitation number, $\sigma = 0.106$, and two flow coefficients are compared in figure 11. As in the case of the tangential forces, a decrease in the flow coefficient clearly causes changes in the normal force. The number of zero crossings increase with a decrease in the flow coefficient and an additional region of positive (destabilizing) force occurs around $\omega/\Omega = 0.1$. Another significant effect caused by decreasing the flow coefficient is the appearance of a negative peak in the normal force in a region of positive whirl; at $\phi = 0.049$, $\sigma = 0.106$ this peak occurs around $\omega/\Omega \approx 0.2$. It is also observed at lower flow coefficient that the normal force tends to remain negative over a longer range of positive whirl frequencies. A comparison similar to that of figure 11 is shown in figure 12, but at the lower cavitation number $\sigma = 0.098$. An increase in the number of zero crossings of the force is observed at the lower flow coefficient. A positive (destabilizing) peak appears at $\omega/\Omega \approx 0.1$ for the lower flow coefficient at this cavitation number and along with a negative peak at $\omega/\Omega \approx 0.2$.

DISCUSSION

The results presented in this paper show that cavitation has a significant effect on inducer rotordynamic forces. The destabilizing rotordynamic effects could lead to failure of the device in which the inducer is being used. It is therefore important to gain a fundamental understanding of the nature of these forces, in order to facilitate changes in the design and/or operating conditions of the machine.

A simple helical inducer was chosen for these preliminary tests. The effect of the geometry of inducers of this type on the cavitation performance have been reported previously (Acosta, 1958). The mechanism of head breakdown has also been studied by researchers such as Jakobsen (1964).

The influence of the flow coefficient on non-cavitating steady forces has been reported earlier (Bhattacharyya et al. 1992). It was shown that the presence of a downstream asymmetry causes significantly large steady forces due to the occurrence of a downstream flow reversal. The downstream reverse flow consists of high energy fluid (on which pumping work has already been done) and the asymmetry causes a net radial force. It was demonstrated that the imposition of a uniform downstream condition (with a perforated screen) led to a near zero lateral force on the inducer (Bhattacharyya et al. 1992). The current experiments with cavitation were conducted with the same downstream asymmetry which is inherent to the system. This is the cause of the large non-cavitating steady force seen in figures 5 and 6. However, it may be noted that the downstream reversal for $\phi = 0.074$ is probably only incipient since previous flow visualization on the hub did not reveal re-entry flows on the hub (there was no observable upstream swirling backflow either). Furthermore, the occurrence of cavitation at this higher flow rate actually results in a lower net steady force. It may be speculated that this occurs because of the lower pumping work being done on the fluid because of cavitation. In the case of the lower flow coefficient, the steady force always remains high regardless of the extent of cavitation.

The unsteady force data suggest that flow reversals can also have significant consequences for rotordynamic forces. For non-cavitating flow the tangential forces are higher in magnitude at lower flow coefficients and are destabilizing for positive whirl at both flow coefficients. The non-cavitating tangential force, however shows a destabilizing peak for positive whirl at $\omega/\Omega = +0.1$ and a negative peak at $\omega/\Omega = +0.2$ for the lower flow coefficient. A similar observation was made on non-cavitating inducers by Arndt and Franz (1986). A more dramatic effect of the flow coefficient is observed in cavitating flow. In the case of the inducer tested, the effect of lowering the flow coefficient increased the region of destabilization (positive F_t) for positive whirl. Furthermore, the effect of a decreased flow did not change the location of the peak, but rather led to an increase in its magnitude. For negative whirl, the higher flow coefficient was more destabilizing. This is an interesting observation especially when the current results are compared to the data obtained previously by Karyeaclis et al. (1989) on a four bladed inducer (called the SEP inducer) with a hub which increases substantially between inlet and discharge. In the case of the SEP inducer, the tangential forces were less destabilizing for the lower coefficient for positive whirl frequencies, unlike the current results. Karyeaclis et al. (1989) argued that for a given cavitation number, larger forces could be expected at the higher flow coefficient because it is closer to the performance breakdown point. Those results were based

on the limited amount of force data available at that time. The current results do not show the same trend; thus it appears that the *geometry* of the inducer has a significant effect on the rotordynamic forces. Further, the current results show a tangential force peak at $\omega/\Omega = +0.2$ rather than at $\omega/\Omega = +0.5$ observed for the SEP tests. In Karyeaclis et al. (1989) it was argued that the peak at $\omega/\Omega = +0.5$ was a sympathetic resonance with the fluid behind the inducer which rotates at half the shaft speed. In the current tests, however, the peak occurs at much less than half the shaft speed. In the case of the normal forces, the effect of a reduction in the flow coefficient was an increase in the number of positive and negative peaks. These differences in the characteristics of the rotordynamic forces with whirl frequencies under cavitating conditions probably stem from the differences in the internal flows and reverse flow patterns caused by the geometry differences in inducers..

The effect of cavitation on the tangential forces at a given flow coefficient is significant. It is observed that for decreasing cavitation numbers, the magnitude of the peak in the force at $\omega/\Omega = +0.2$ increases and becomes narrower. Thus the range of destabilizing forces decreases. This is the reverse of the trend to that observed by Karyeaclis et al. (1989) for the SEP inducer where larger forces were accompanied by larger instability regions. Also, in the case of the current inducer the tangential forces with increasing cavitation become increasingly stabilizing for negative whirl.

Another important observation is that the data for F_t and F_n as a function of ω/Ω do not exhibit the kind of quadratic functional behavior which is normally assumed in many rotordynamic models. Rather, as has been reported previously (Karyeaclis et al., 1989) much higher order polynomials would be required to approximate the forces. Thus the representation of the components of the rotordynamic matrix $[A]$ (as given in equation 4) does not hold for the cavitating inducer. Consequently, the generalized stiffness, damping and inertia matrices for the inducer cannot be determined. Instead, rotordynamic analysis of the inducer must include fluid-induced forces which are more general functions of the whirl frequency ratio.

CONCLUSIONS

(1) Cavitation has important consequences for fluid-induced rotordynamic forces generated by inducers. These forces can become destabilizing at both positive and negative whirl frequencies.

(2) The rotordynamic forces do not exhibit a quadratic functional behavior and hence the conventional generalized stiffness, damping and inertia matrices cannot be determined.

(3) The internal flow patterns and flow reversals associated with reduced flow coefficients appear to have a significant bearing on these forces. The flow patterns are, in turn, dependent on the inducer geometry and the dependence of the forces on the extent of cavitation must be included in design considerations.

Given that analytical techniques are, as yet, unable to predict unsteady cavitating forces in turbomachinery, the experimental data obtained in the current research provides an appropriate starting point for the understanding of these complex forces in axial flow inducers.

ACKNOWLEDGEMENT

The authors would like to thank the NASA George C. Marshall Space Flight Center for sponsoring this project under contract no. NAG8-118, Henry L. Stinson, contract monitor..

REFERENCES

Acosta, A.J., 1958, "An Experimental Study of Cavitating Inducers," *Proc. of 2nd Symp. on Naval Hydrodynamics,* Washington D.C., pp. 533-557.

Acosta, A.J., 1993, "Flow in Inducer Pumps, An Aperçu," *Proc. of the 4th Int. Symp. on Trans. Phenomena and Dyn. of Rot. Mach.,* Honolulu, Vol. A., pp. 1-13.

Arndt, N., and Franz, R., 1986, "Observations of Hydrodynamic Forces on Several Inducers including the SSME LPTOP," *Calif. Inst. of Tech., Div. of Appl. Sci. Report No. E249.3,* Pasadena, California.

Bhattacharyya A., Acosta A.J., Brennen C.E., and Caughey, T.K., 1992, "The Formation of Backflow and its Consequences on the Lateral Forces on Axial Flow Impellers," *Abstracts of the ASME Fluids Engg, Conf.,* Los Angeles, FED-Vol. 133, pp. 237-239.

Bhattacharyya A., Acosta A.J., Brennen C.E., and Caughey, T.K., 1993, "Observations on Off-Design Flows in Axial Flow Inducers," *Proc. of the Pumping Mach. Symp. at the ASME Fluids Engg. Conf.,* Washington D.C., June 20-24, 1993, FED-Vol. 154, pp. 135-141.

Franz R., 1989, "Experimental Investigation of the Effect of Cavitation on the Rotordynamic Forces on a Whirling Centrifugal Pump Impeller," Ph.D. Thesis, Calif. Inst. of Tech., Pasadena, CA.

Guinzburg A., 1992, "Rotordynamic Forces Generated by Discharge-to-Suction leakage Flows in Centrifugal pumps," Ph.D. Thesis, Calif. Inst. of Tech., Pasadena, CA.

Jakobsen, J.K., 1964, "On the Mechanism of Head Breakdown in Cavitating Inducers," ASME *J. of Basic Eng.,* June 1964, pp. 291-305.

Jery, B., 1986, "Experimental Study of Unsteady Hydrodynamic Force Matrices on Whirling Centrifugal Pump Impellers," Ph.D. Thesis, Calif. Inst. of Tech., Pasadena, CA.

Kamijo, K.,, Shimura T., Watanabe M., 1977, "An Experimental Investigation of Cavitating Inducer Instability," *Proc. of the ASME Winter Annual Meeting ,* Atlanta, Georgia, 1977.

Karyeaclis, M.P., Miskovish, R.S., and Brennen, C.E., 1989. Rotordynamic Tests in Cavitation of the SEP Inducer. Calif. Inst. of Tech., Div. of Eng. and Appl. Sci. Report no. E200.27.

Lakshminarayana, B., 1972, "Visualization Study of Flow in Axial Flow Inducer," ASME *J. of Basic Eng.*, pp. 777-787.

Lakshminarayana, B., 1982, "Fluid Dynamics of Inducers - A Review," ASME *J. of Fluids Eng.*, vol. 104, pp. 411-427.

Rosenmann, W., 1965. Experimental Investigations of Hydrodynamically Induced Shaft Forces with a Three Bladed Helical Inducer. *Proc. ASME Symp. on Cavitation in Turbomachinery*, pp. 172-195.

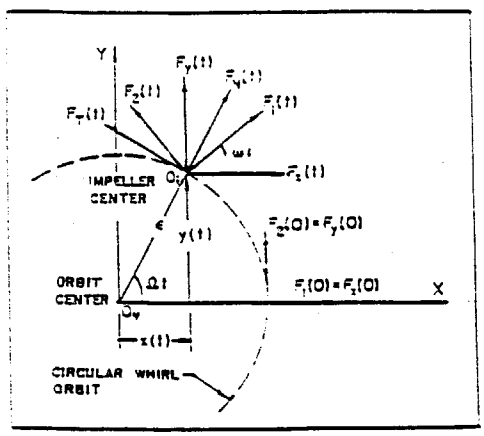

FIG. 1. SCHEMATIC SHOWING LABORATORY AND ROTATING REFERENCE FRAMES AS WELL AS ROTORDYNAMIC FORCES.

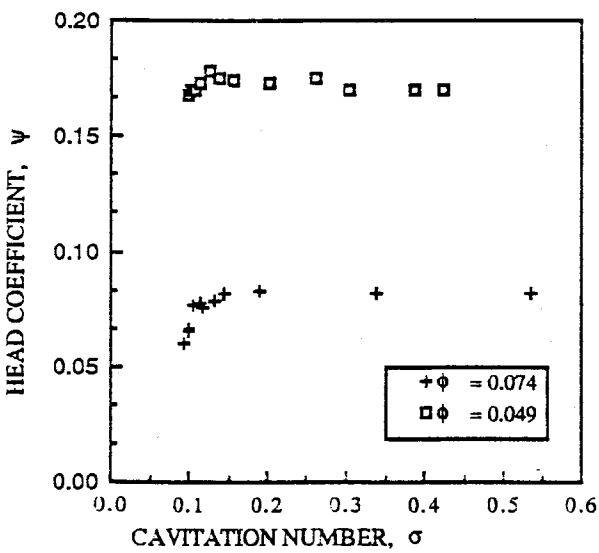

FIG. 2. CAVITATION CHARACTERISTICS OF THE INDUCER AT 3000 RPM.

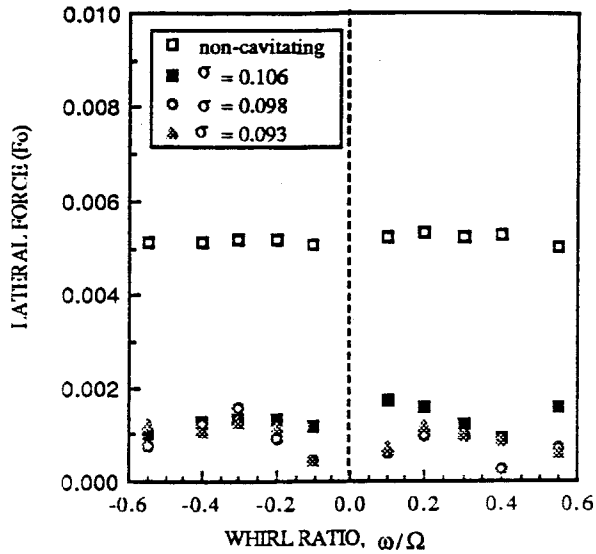

FIG. 3. LATERAL FORCE ON THE INDUCER AT FLOW COEFFICIENT ϕ = 0.074 FOR VARIOUS CAVITATION NUMBERS.

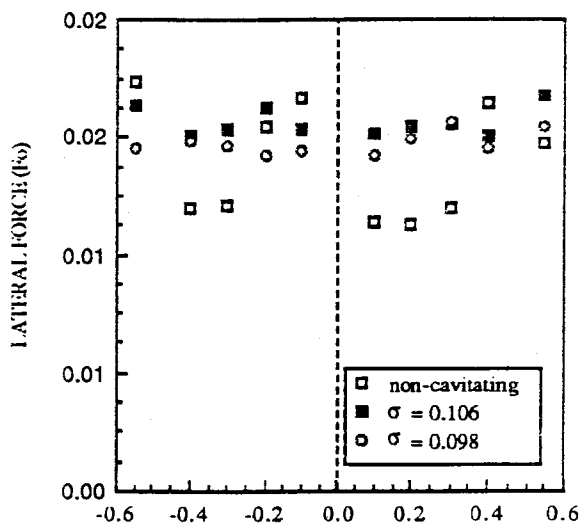

FIG. 4. LATERAL FORCE ON THE INDUCER AT FLOW COEFFICIENT ϕ = 0.049 FOR VARIOUS CAVITATION NUMBERS.

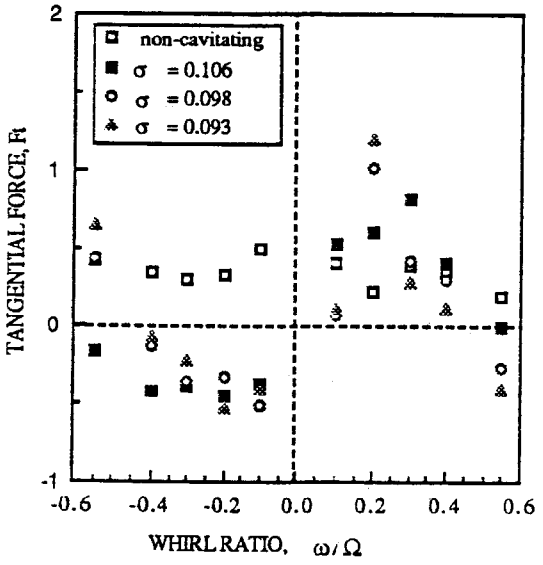

FIG. 5. TANGENTIAL FORCE ON INDUCER AT FLOW COEFFICIENT ϕ = 0.074 FOR VARIOUS CAVITATION NUMBERS.

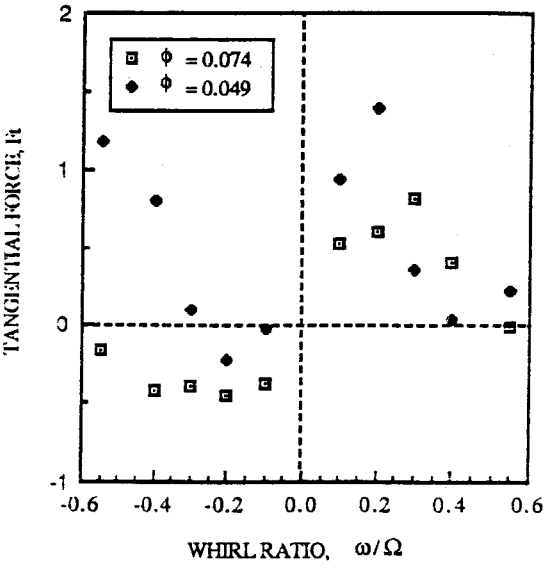

FIG. 7. COMPARISON OF THE TANGENTIAL FORCE ON THE INDUCER AT A CAVITATION NUMBER σ = 0.106 FOR TWO FLOW COEFFICIENTS.

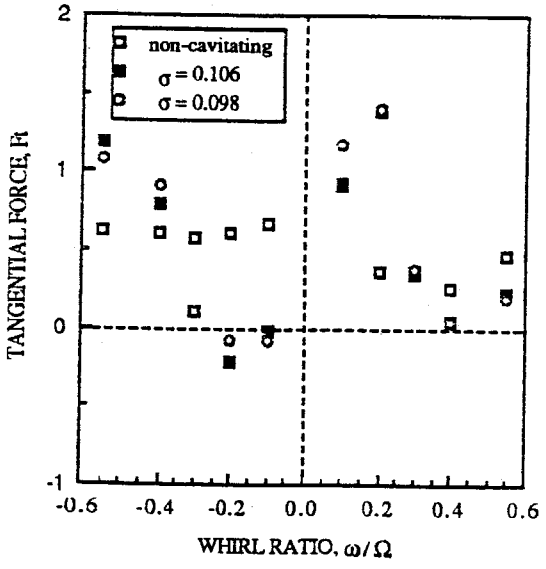

FIG. 6. TANGENTIAL FORCES AT A FLOW COEFFICIENT ϕ = 0.049 FOR VARIOUS CAVITATION NUMBERS.

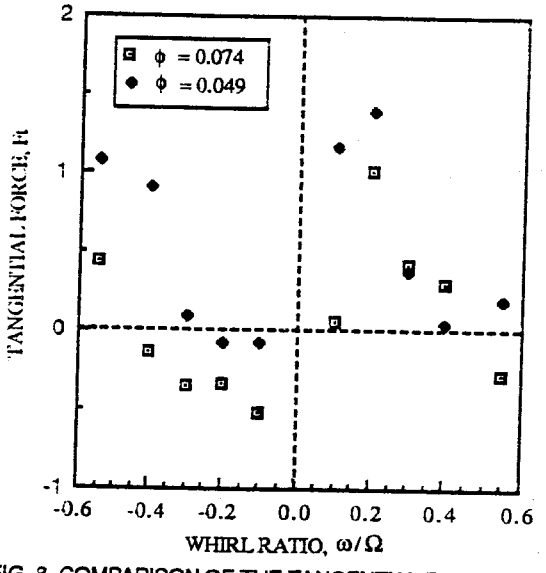

FIG. 8. COMPARISON OF THE TANGENTIAL FORCE ON THE INDUCER AT CAVITATION NUMBER σ = 0.098 FOR TWO FLOW COEFFICIENTS.

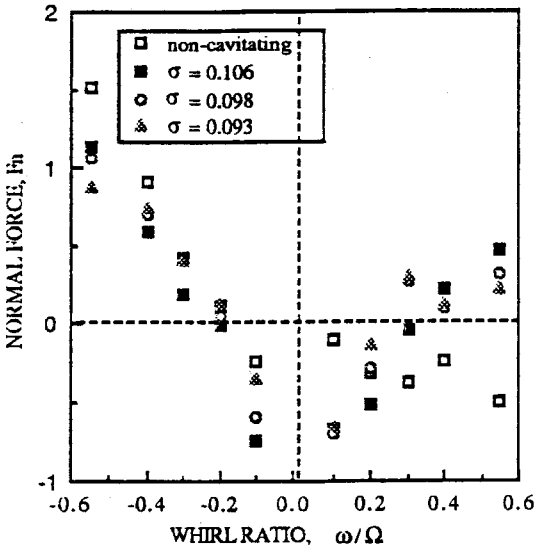

FIG. 9. NORMAL FORCES AT FLOW COEFFICIENT ϕ = 0.074 FOR VARIOUS CAVITATION NUMBERS.

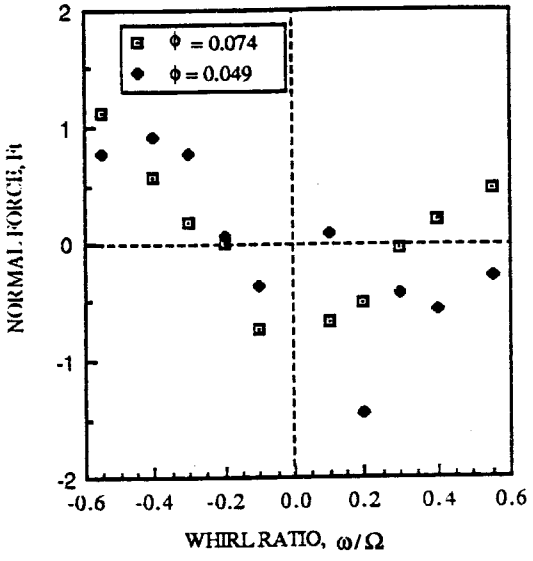

FIG. 11. COMPARISON OF THE NORMAL FORCES AT A CAVITATION NUMBER σ = 0.106 FOR TWO FLOW COEFFICIENTS.

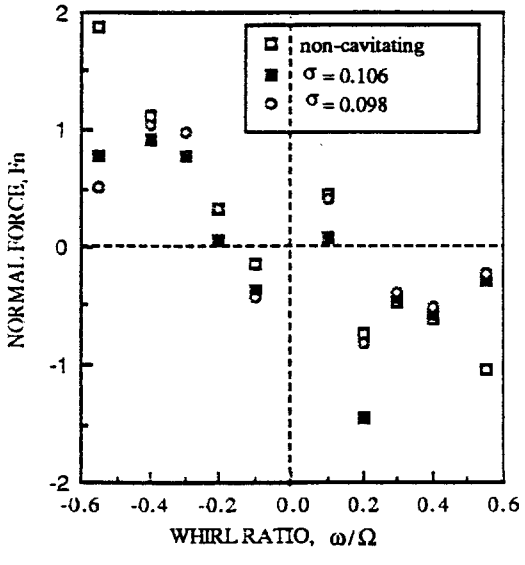

FIG. 10. NORMAL FORCES AT FLOW COEFFICIENT ϕ = 0.049 FOR VARICUS CAVITATION NUMBERS.

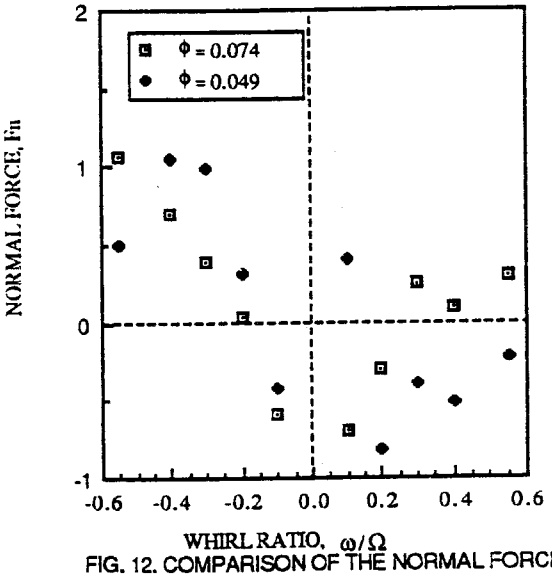

FIG. 12. COMPARISON OF THE NORMAL FORCES AT A CAVITATION NUMBER σ = 0.098 FOR TWO FLOW COEFFICIENTS.